International Journal of Nanomedicine

Dovepress
open access to scientific and medical research

Open Access Full Text Article

ORIGINAL RESEARCH

Carbon Dots Derived from *Curcumae Radix* and Their Heartprotective Effect

Liyang Dong[1,*], Yafang Zhao[1,*], Juan Luo[1,2], Xiaopeng Li[1], Shuxian Wang[1], Menghan Li[1], Peng Zou[1], Hui Kong[1], Qingguo Wang[1], Yan Zhao[1], Huihua Qu[1]

[1]School of Traditional Chinese Medicine, Beijing University of Chinese Medicine, Beijing, People's Republic of China; [2]Institute of Precision Medicine, Peking University Shenzhen Hospital, Shenzhen, People's Republic of China

*These authors contributed equally to this work

Correspondence: Qingguo Wang; Yan Zhao, Email wangqg8558@sina.com; zhaoyandr@163.com

Background: Acute myocardial infarction (AMI) is a common cardiovascular disease in clinic. Currently, there is no specific treatment for AMI. Carbon dots (CDs) have been reported to show excellent biological activities, which hold promise for the development of novel nanomedicines for the treatment of cardiovascular diseases.

Methods: In this study, we firstly prepared CDs from the natural herb *Curcumae Radix* Carbonisata (CRC-CDs) by a green, simple calcination method. The aim of this study is to investigate the cardioprotective effect and mechanism of CRC-CDs on isoproterenol (ISO) -induced myocardial infarction (MI) in rats.

Results: The results showed that pretreatment with CRC-CDs significantly reduced serum levels of cardiac enzymes (CK-MB, LDH, AST) and lipids (TC, TG, LDL) and reduced st-segment elevation and myocardial infarct size on the ECG in AMI rats. Importantly, cardiac ejection fraction (EF) and shortening fraction (FS) were markedly elevated, as was ATPase activity. In addition, CRC-CDs could significantly increase the levels of superoxide dismutase (SOD), reduced glutathione (GSH), catalase (CAT), and reduce the levels of malondialdehyde (MDA) and reactive oxygen species (ROS) in myocardial tissue, thereby exerting cardioprotective effect by enhancing the antioxidant capacity of myocardial tissue. Moreover, the TUNEL staining image showed that positive apoptotic cells were markedly declined after CRC-CDs treatment, which indicate that CRC-CDs could inhibit cardiomyocyte apoptosis. Importantly, The protective effect of CRC-CDs on H_2O_2 -pretreated H9c2 cells was also verified in vitro.

Conclusion: Taken together, CRC-CDs has the potential for clinical application as an anti-myocardial ischemia drug candidate, which not only provides evidence for further broadening the biological application of cardiovascular diseases, but also offers potential hope for the application of nanomedicine to treat intractable diseases.

Keywords: acute myocardial infarction, Curcumae Radix Carbonisata, carbon dots, oxidative stress

Introduction

Cardiovascular disease (CVD) is one of the most important causes of death worldwide, accounting for 31.5% of deaths and more than twice the number of cancers, according to epidemiological data from the Global Burden of Disease Study 2013 (GBD 2013).[1] However, acute myocardial infarction (AMI) is the most common form of CVD, with a high incidence in the last few decades. By 2030, 23 million people in China will be affected by AMI, making a sizeable section of the population susceptible to AMI accidents.[2] AMI is a frequent and common disease with high morbidity and mortality, which not only brings physical and mental suffering to patients, but also imposes a huge economic burden on society and families.[3]

Although the pathogenesis of AMI is unknown, studies have shown that oxidative stress and apoptosis play an important role in the pathogenesis of AMI. Studies have shown that reactive oxygen species (ROS) induced oxidative stress is a major cause of apoptosis in myocytes.[4] Excessive ROS production can break down intracellular macromolecules, such as proteins

Received: 28 October 2023
Accepted: 27 March 2024
Published: 8 April 2024

Graphical Abstract

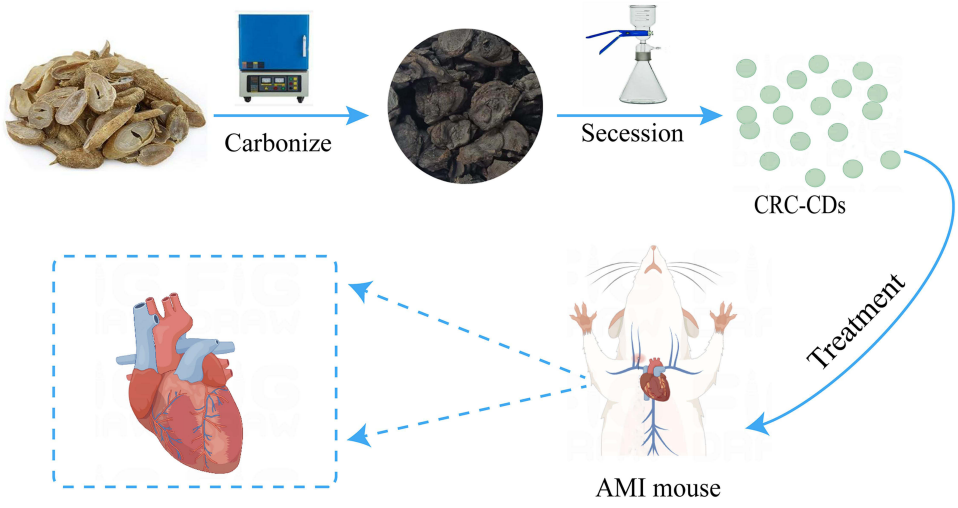

and DNA, leading to apoptosis. Therefore, regulation of ROS levels and modulation of the apoptotic cascade is considered a key therapeutic strategy for the treatment of AMI.[5,6]

Treatment for AMI usually involves revascularisation of the occluded artery, but this often leads to reperfusion injury and arrhythmias.[7,8] Commonly used drugs for AMI patients in clinical practice currently include β-adrenergic receptor antagonists and the class III drug amiodarone, which improve survival; however, there is no evidence of their pharmacological efficacy in the acute phase of AMI.[9] Numerous experimental studies have shown that traditional Chinese herbal medicines are more effective in the treatment of cardiovascular diseases, including ischaemic heart disease, and that the natural substances in herbal medicines are not only green and safe, with few side effects, but also have strong anti-oxidant and anti-apoptotic properties.[10–12]

Nanotechnology has been a hot topic of research in recent years and has had a huge impact on the innovation and development of medicine, including nano-pharmaceuticals, nano-biomaterials and nano-biosensors.[13–15] Meanwhile, nanotechnology has great potential for the treatment and detection of cardiovascular diseases. For example, based on the good electrical, thermal and optical properties of carbon nanotubes, carbon nanotube nanostructured immunosensors have been developed for the detection of cardiac troponin T (cTnT), which is of great importance for the early diagnosis and prevention of AMI.[16,17] Moreover, Kumar.et aligned PCL-Gelatin coaxial nanofibre patches were prepared using human induced pluripotent stem cell-derived cardiomyocytes (hiPSC-CMs) and electrostatic spinning, which promotes the maturation of hiPSC-CMs and the formation of functional syncytia in cardiac tissue, which contributes to the regeneration and repair of myocardium.[18] Hardy et al showed that both l-typeCa^{2+} channel activity could be attenuated and excessive oxidative stress responses in cardiac myocytes reduced by simultaneous delivery of peptides and curcumin into multifunctional poly (glycidyl methacrylate) (PGMA) nanoparticles.[19]

Carbon dots (CDs), a novel carbon nanomaterial with a characteristic size of less than 10 nm and containing different organic functional groups, have inspired extensive research in a wide range of disciplines, including physics,[20] chemistry[21] and medicine,[22] due to their excellent properties such as good biocompatibility, stable optical properties and non-toxicity. In the team's previous research, we identified a variety of CDs from carbonised herbs that have a variety of haemostatic, anti-inflammatory, sedative and antibacterial effects.[23–27]

Curcumae Radix, named yujin in Chinese, is a traditional herb that has been used for thousands of years in China, especially in cardiovascular diseases.[28] It has been shown that nanoparticles extracted from traditional herbs, such as Scutellaria baicalensis and Euphorbia fischeriana, have a good protective effect against myocardial infarction,[29,30] while

the application of Curcumae Radix carbon dots has not been reported before. Based on this, the possibility of controlling or treating CDs in acute myocardial infarction has become the focus of current research, which is worth undertaking.

In this study, a new type of CDs (CRC-CDs) was prepared by a green one-step calcination method using Curcumae Radix (CR) as the sole carbon source. The physical morphology and optical properties of CRC-CDs were characterized by electron microscopy and optical instrumentation, and their functional groups and coordination bonds were analyzed. Animal experiments were conducted using an isoproterenol induced acute myocardial infarction (AMI) model in rats to investigate whether CRC-CDs pretreatment could improve myocardial ischemia and prevent the occurrence of myocardial infarction, thus exerting a cardioprotective effect.

Materials and Methods

Chemicals

Curcumae Radix was purchased from Beijing Qiancao Herbal Pieces Co., Ltd (Beijing, China). Dialysis membranes with a molecular weight of 1000 Da were purchased from Beijing Ruida Henghui Technology Development Co., Ltd (Beijing, China). Cell counting kit (CCK-8) and other analytical grade chemical reagents were obtained from Beijing BioDee Biotechnology Co., Ltd (Beijing, China). Propranolol hydrochloride was purchased from Beijing Zhengcheng Biotechnology Co., Ltd (Beijing, China). Isoproterenol hydrochloride was purchased from Bairdi Biotechnology Co., Ltd (Beijing, China). All the experiments were conducted using deionized water.

Animals and Experimental Protocols

Animals

All the experimental procedures were performed in agreement with the Regulations for the Administration of Affairs Concerning Experimental Animals approved by the State Council of People's Republic of China. The experimental procedures were approved by the Committee of Ethics of Animal Experimentation of Beijing University of Chinese Medicine (BUCM) and by the Health Guide for Care and Use of Laboratory Animals. Rat cardiomyocyte H9c2 cells were purchased with Peking Union Cell Bank (Beijing, China). Male adult Sprague Dawley (SD) rats of average weight, 220 grams, were purchased from SiPeiFu Biotechnology Co., Ltd (Beijing, China) and were housed in the Laboratory Animal Center of Beijing University of Chinese Medicine at 24.0 ± 1.0 °C with 55–65% relative humidity under a 12 h light/dark cycle and allowed to feed ad libitum.

Experimental Protocols

Sprague-Dawley (SD) rats totaling 50 were split into the following six groups at random (n=8, in each group), and the medication was administered as follows:

Control group (Control group): the animals were received only saline for 14 days.

ISO induced AMI group (ISO group): the animals were received saline for 14 days and administered with ISO (85 mg/kg, Multiple subcutaneous injections) for 2 days on the 13th and 14th day, model success represented by significant arch-back elevation of the ST segment on ECG.

ISO combined with Propranolol group (Propranolol group): The animals were pretreated with propranolol hydrochloride for 14 days (10 mg/kg) and administered with ISO (85 mg/kg, Multiple subcutaneous injections) for 2 days on the 13th and 14th day.

ISO combined with low-dose CRC-CDs pretreatment group (Low-dose CRC-CDs group): the animals were treated with 1.75 mg/kg/d of CRC-CDs for 14 days and administered with ISO (85 mg/kg, Multiple subcutaneous injections) for 2 days on the 13th and 14th day.

ISO combined with medium-dose CRC-CDs pretreatment group (Medium-dose CRC-CDs group): the animals were treated with 3.5 mg/kg/d of CRC-CDs for 14 days and administered with ISO (85 mg/kg, Multiple subcutaneous injections) for 2 days on the 13th and 14th day.

ISO combined with high-dose CRC-CDs pretreatment group (High-dose CRC-CDs group): the animals were treated with 7 mg/kg/d of CRC-CDs for 14 days and administered with ISO (85 mg/kg, Multiple subcutaneous injections) for 2 days on the 13th and 14th day.

Preparation and Characterization of CRC-CDs

Preparation of CRC-CDs

According to earlier reports, CRC-CDs were created using the one-step pyrolysis technique at a high temperature using CRC as the carbon source. As a first step, 400 g Curcumae Radix was fixed in crucibles, fixed with the top and foil paper were closed to make a tight fit seal, at this time calcined in a furnace of muffle (TL0612, Beijing Zhong Ke Anbo Innovation Co., Ltd., China) for 1h at 360°C to deliver CRC. After the temperature has cooled to room temperature, CRC was crushed with a micro pulveriser. The resulting uniform black residues were finely crushed and cooked in water twice for one hour each, each time at a temperature of 100°C. To extract the CRC-CDs, the resulting solution was first filtrated through a 0.22 μm cellulose acetate membrane and then dialyzed for 7 days against DW using a 1000-Da membrane.

Characterisation of CRC-CDs

TEM (Tecnai G220; FEI Company, USA) was used to analyze the microstructure, particle size distribution, and morphology of CRC-CDs at a 100 kV accelerating voltage. HRTEM (JEN-1230; Japan Electron Optics Laboratory; Japan) was used to study atomic lattice fringes and other structural features. Using UV-Vis (CECIL, Cambridge, UK) and fluorescence (F-4500, Tokyo, Japan) spectroscopy, respectively, the ultraviolet-visible (UV-Vis) spectrum and fluorescence characteristics were recorded and quantified. XRD (D8-Advanced X-ray diffractometer, Bruker AXS, Karlsruhe, Germany) was performed with Cu K-alpha radiation. The surface composition of CRC-CDs was investigated using X-ray photoelectron spectroscopy (XPS) on an X-ray photoelectron spectrometer (ESCALAB 250Xi, Thermo Fisher Scientific, MA, USA) with a mono X-ray source AlK 150 W. The composition of functional groups on the surface of CRC-CDs between 400 and 4000 cm^{-1} was identified using Fourier transform infrared (FTIR) spectroscopy (Thermo, California, USA).

Echocardiography

The rats in each group were anesthetized with 10% chloral hydrate intraperitoneally (300 mg/ kg) and then prepared for skin fixation. Echocardiography was performed on the rats by a Visual Sonics Vevo 2100 ultra-high resolution small animal ultrasound imaging system equipped with a 10 MHz linear array ultrasound transducer. The left ventricular end-systolic internal diameter (LVESD) and left ventricular end-diastolic internal diameter (LVEDD) were measured separately and the left ventricular ejection fraction (EF) and shortening fraction (FS) were calculated.

Evaluation of Heart Weight Index

After the final experiment, the rats were anaesthetised, blood was taken and the serum was separated; the rat hearts were quickly removed and the residual blood was washed away with ice-cold saline, the large blood vessels and connective tissue were cut away, blotted on filter paper, weighed and stored at −80°C. The heart weight index (HWI) was calculated as HWI = heart weight (HW) /body weight (BW).

Histological Examination of Myocardium

Immediately after the sacrifice of the rats, the heart tissues were removed and fixed in 10% formalin solution. The sections were then dehydrated in an ethanol gradient, embedded in paraffin, and stained with hematoxylin and eosin (HE) staining reagent and Masson staining reagent, and the pathological changes in each group of heart tissue were observed using a light microscope (Nikon, Tokyo, Japan).

Tissue Necrosis Assessment

Tissue necrosis was assessed by Evans blue/triphenyltetrazolium Chlorinated (TTC) tissue enzyme staining technique. After removal of the rat heart, the left ventricle was transected into 5 slices perpendicular to the long axis of the heart and incubated in 1% TTC solution for 15 min at 37°C and protected from light. TTC stained greyish white are infarcted areas (IS) and red are non-infarcted areas (NIS).

$$\text{Percentage of infarction} = \text{area of infarcted area}/\text{area of left ventricle} \times 100\%.$$

Serum Biochemical Analysis

After anaesthesia in rats, blood was taken from the abdominal aorta, centrifuged at 4°C for 10 min at 3500 $r \cdot min^{-1}$ and serum was obtained. Then, the serum levels of lactate dehydrogenase (LDH), creatine kinase isoenzyme (CK-MB), aspartate aminotransferase (AST), total cholesterol (TC), triglycerides (TG), low density lipoprotein (LDL) and high density lipoprotein (HDL) were measured by a fully automated biochemical analyser.

Assessment of Oxidative Stress in Myocardial Tissue

The MDA levels, as well as the SOD, CAT, and GSH-Px activities, were measured in myocardial tissue. Following the manufacturer's instructions, all indicators were measured using a microplate reader with the appropriate detection kits.

Myocardial Na^+-K^+-ATPase and Ca^{2+}-Mg^{2+}-ATPase activities assay

Rat myocardial tissue homogenate supernatant, Following the manufacturer's instructions, the activities of the heart's Na^+-K^+-ATPase and Ca^{2+}-Mg^{2+}-ATPase were measured spectrophotometrically using the appropriate commercial diagnostic kits.

TUNEL Assay

Rat myocardial tissue was fixed in 4% paraformaldehyde, rinsed in double-distilled water and embedded in paraffin, and sections of 2–3 μm thickness were prepared and incubated for 60 min with drops of TUNEL reaction solution. DAPI-covered cells to re-stain nuclei. Drops of anti-fluorescence quencher were added to seal the slices, apoptosis-positive cell counts were observed under a light microscope and the apoptosis rate was calculated. Apoptosis rate (%) = number of apoptotic cells TUNEL / number of total cells DAPI × 100%.

Cell Culture and Cytotoxicity

H9c2 cells were cultured in high glucose DMEM containing 10% fetal bovine serum and 1% penicillin/streptomycin in an incubator at 37°C with 5% CO_2, 95% air. Cells were passaged when the cell adhesion rate reached 80%, every 2–3 d. Logarithmic growth stage H9c2 cells were taken for subsequent experiments. CCK-8 kit to detect cytotoxicity of CRC-CDs versus H9c2, which were purchased from Procell Life Science & Technology Co. Ltd. (Wuhan, China). H9c2 cells were inoculated in 96-well plates at a density of 5×10^4 cells/each 100 μL/well and cultured for 24 h. Each well was replaced with 100 μL of medium containing graded concentrations of CRC-CDs (1000, 500, 250, 125, 62.50, 31.25, 15.63 μg/mL). After washing the plate three times with PBS, 10 μL of CCK-8 reagent was added to each well 4 h incubation. A microplate reader (Biotek, Vermont.) was used to measure the absorbance of each well at 450 nm. Cell viability is calculated using the following formula: Cell Viability (% of control) = (Ae-Ab)/(Ac-Ab) × 100 (Ae, Ab and Ac indicate the absorbance at 450 nm for the experimental, blank and control groups respectively).

H_2O_2-induced injury model H9c2 cells and drug therapy

H9c2 cells were cultured under the same conditions as above and randomly divided into five groups: control group (control, normal DMEM medium culture); H_2O_2 hypoxia model group (model, incubated in DMEM medium containing 10% H_2O_2 for 2 h); Low-dose CRC-CDs treatment group (Cells were precultured in normal DMEM medium containing 31.25 $\mu g.mL^{-1}$ CRC-CDs for 24 h, with other operations were consistent with the model group); Medium-dose CRC-CDs treatment group (Cells were precultured in normal DMEM medium containing 62.5 $\mu g.mL^{-1}$ CRC-CDs for 24 h, with other operations were consistent with the model group); High-dose CRC-CDs treatment group (Cells were precultured in normal DMEM medium containing 125 $\mu g.mL^{-1}$ CRC-CDs for 24 h, with other operations were consistent with the model group). Degree of cell damage LDH and CK levels were determined for each gradient of cell supernatant using the LDH and CK assay kit, following the manufacturer's instructions.

Statistical Analysis

Statistical analyses for all experiments were performed using IBM SPSS Statistics (version 26) for statistical analysis. The mean ± standard deviation (SD) provided for data with normal distribution and homogeneity of variance. One-way analysis of variance (ANOVA) was performed to compare differences between groups. Data with non-normal distribution Non-normally distributed data were analysed using non-parametric statistics, using the Kruskal–Wallis test and a post-hoc test, with $P < 0.05$ and $P < 0.01$ considered as differences to be statistically significant.

Results

Characterization of CRC-CDs

TEM and HRTEM were used to examine the morphology and particle size distribution of CRC-CDs. The TEM images (Figure 1A) showed that the CRC-CDs were spherical with monodisperse quasi-spherical structure and particle size distribution in the range of 0.5~3.5 nm (Figure 1C). HRTEM images (Figure 1B) show that the lattice spacing of CRC-CDs is 0.216 nm and their structure is similar to the crystal skeleton of graphite.[31] The identifiable diffraction peak in the XRD spectrum (2θ = 21.87°) indicates that the CRC-CDs are amorphous carbon phases, which is consistent with the HRTEM image (Figure 1D).[32]

The luminescence properties of CRC-CDs were investigated. The UV-Vis absorption spectrum (Figure 1E) shows that CRC-CDs has a broad spectrum with no particularly well-defined peaks, but a small absorption peak at 370 nm due to the n -π * electron leap in the conjugated C=O; C=N bond and the aromatic sp^2 structural domain.[33] Analysis of surface functional groups of CRC-CDs by FTIR (Figure 1F). The FTIR spectrum depicts a broad absorption peak at 3440 cm^{-1} caused by the stretching vibration of the O/ N-H bond with peaks at 2919 cm^{-1} and 2850 cm^{-1} in the presence of $-CH_3$ and $-CH_2$ structures. The absorption peak at about 1636 cm^{-1} was identified as C=O, while the peak at 1384 cm^{-1} is a C-N stretching vibration peak.[34,35] Peak located at 1079 cm^{-1} suggested the existing of aromatic alkoxy bonds. FTIR results showed that the surface of CRC-CDs contains including carbonyl and may also contain hydroxyl or amino groups. The fluorescence emission spectrum (Figure 1G) shows excitation at 346 nm, with the highest emission peak at 455 nm. In the excitation wavelength range of 20 nm, as the excitation wavelength increased from 330 nm to 450 nm, the

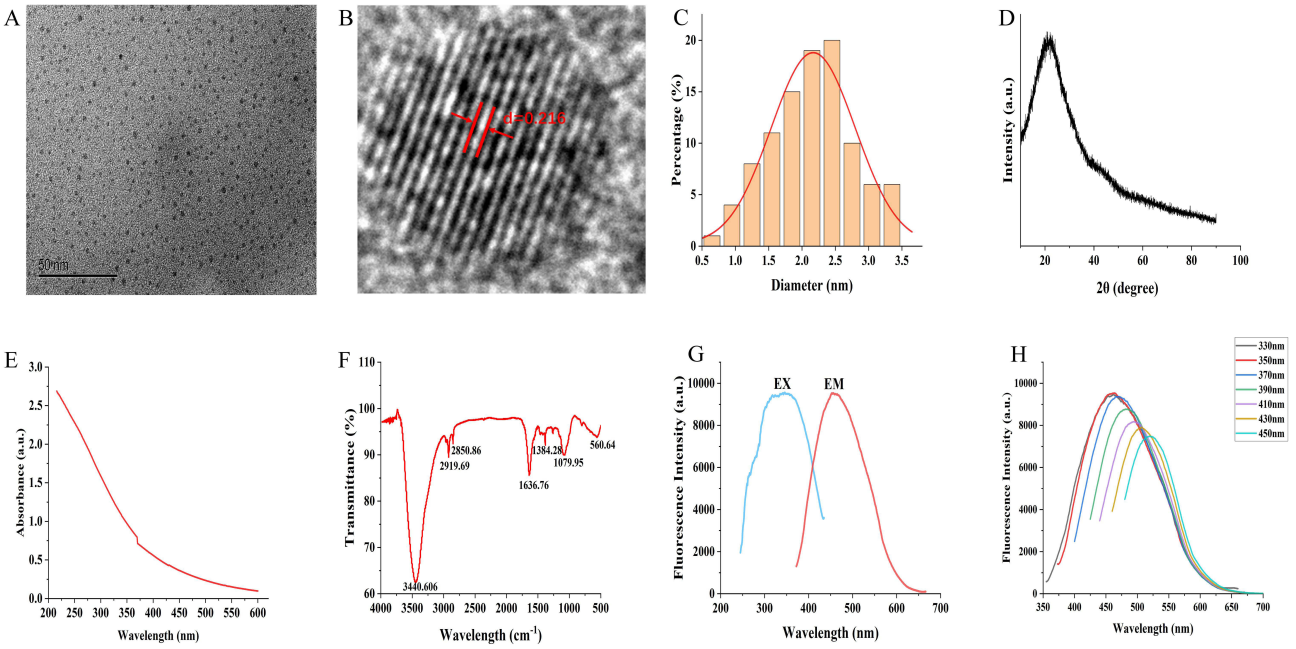

Figure 1 Morphological and optical characterizations of CRC-CDs. (**A**) Transmission electron microscopy (TEM) images. (**B**) High-resolution TEM image of CRC-CDs and lattice spacing (Red arrow indicates) of CRC-CDs (d = 0.216 nm). (**C**) Particle size distribution histogram. (**D**) X-ray diffraction pattern. (**E**) Ultraviolet–visible spectrum. (**F**) Fourier transform infra-red spectrum. (**G**) Fluorescence spectra for excitation and emission. (**H**) Fluorescence spectra of CRC-CDs with different excitation wavelengths.

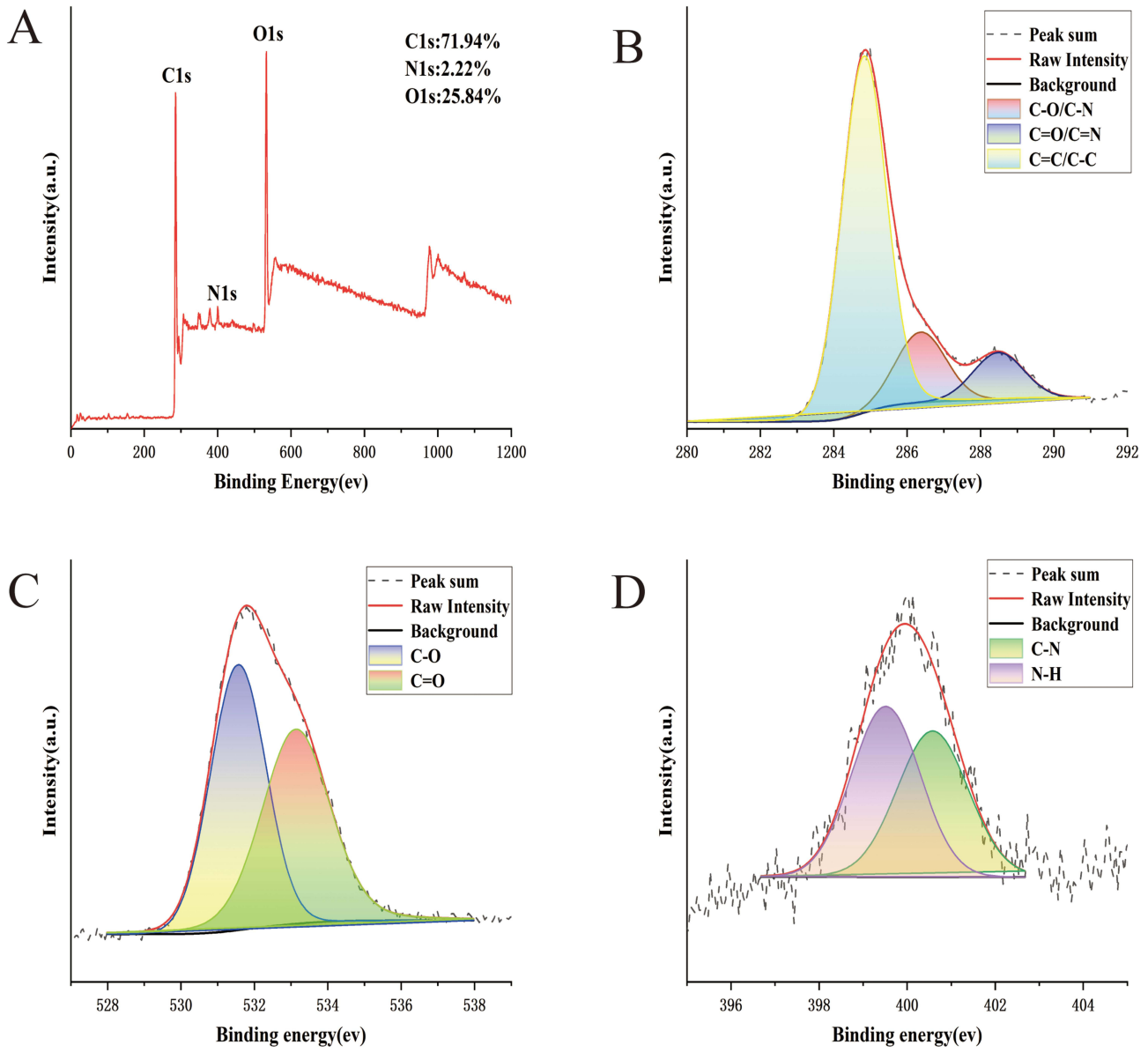

Figure 2 The surface composition and elemental analysis of the prepared CRC-CDs by XPS. (**A**) X-ray photoelectron spectroscopy survey of CRC-CDs. (**B**) C1s. (**C**) O1s. (**D**) N1s.

maximum emission wavelength of CRC-CDs was red-shifted and the fluorescence intensity (Figure 1H) showed a trend of increasing and then decreasing, indicating that CRC-CDs have excitation-related emission properties.

The surface elemental composition and chemical bonding of CRC-CDs were determined by X-ray photoelectron spectroscopy (XPS) and the results showed that CRC-CDs[36] are mainly composed of three elements (Figure 2A), C (71.94%), O (25.84%) and N (2.22%). The C1s (Figure 2B) spectra show distinct peaks at 284.8 eV, 286.3 eV and 288.7 eV, indicating the presence of coordination bonds such as C=C/C-C, C-O/C-N and C=O/C=N. The O1s (Figure 2C) spectra show distinct peaks at 531.56 eV, and 533.13 eV, indicating the presence of coordination bonds such as C-O and C=O. The N1s (Figure 2D) spectra show distinct peaks at 399.45 eV and 400.45 eV, indicating the presence of coordination bonds such as N-H and C-N.[37–39]

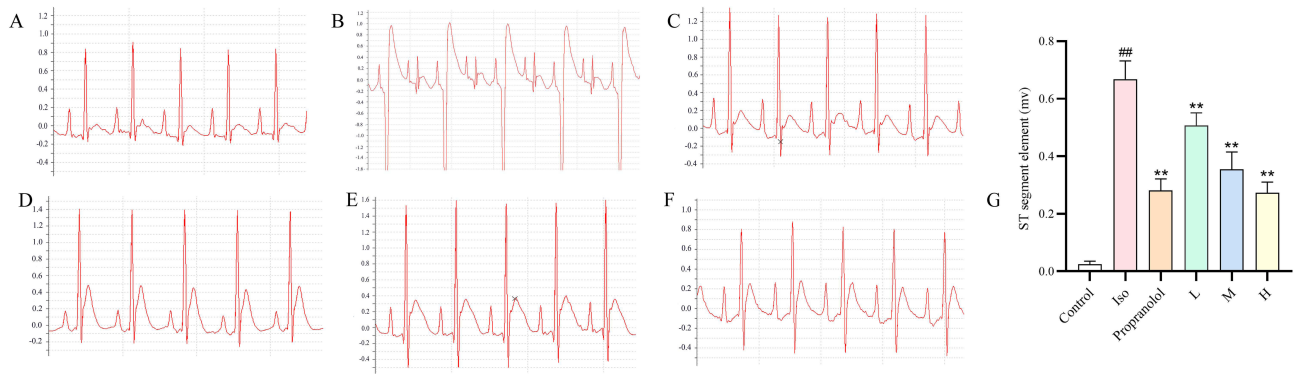

Figure 3 CRC-CDs pretreatment improves cardiac function and reduces ECG ST in rats. (**A**) Control group. (**B**) Iso group. (**C**) Propranolol group. (**D**) Low-dose CRC-CDs group. (**E**) Medium-dose CRC-CDs group. (**F**) High-dose CRC-CDs group. (**G**) Changes in the ST segment of the ECG in each group of rats. Date are represented as means ± SD (n=8). $^{\#\#}P < 0.01$ compared with the control group, $^{**}P < 0.01$compared with the Iso group.

Effect of CRC-CDs on ISO-induced electrocardiographic parameters in rats

ECG abnormalities are the main criteria for confirming the diagnosis of myocardial ischaemia and infarction.[40,41] To evaluate the protective effect of CRC-CDs against myocardial infarction, we measured the changes in the ST segment of the ECG in each group of rats. As shown in Figure 3A, the experimental control rats showed normal ECGs and the Iso-induced AMI group (Figure 3B) showed significantly elevated ST-segments on the ECGs ($P < 0.01$). As shown in Figure 3C–E, The ST-segment was significantly lower in the CRC-CDs pretreatment group (1.75, 3.5 and 7mg/kg, respectively) and the Propranolol group (Figure 3F) compared to the Iso group alone ($P < 0.01$). As shown in Figure 3G, pretreatment with CRC-CDs significantly reduced ECG st-segment elevation in rats with myocardial infarction, thus exerting cardioprotective effects.

Effect of CRC-CDs on ISO-induced echocardiographic parameters in rats

Echocardiography is an important indicator of cardiac function.[42] The protective effect of CRC-CDs on the heart was assessed by measuring the left ventricular end-systolic internal diameter (LVESD) and left ventricular end-diastolic internal diameter (LVEDD) in each group of rats to calculate the left ventricular ejection fraction (EF) and shortening fraction (FS) (Figure 4A–F), respectively.[43] As shown in Figure 4G and H below, the left ventricular ejection fraction (EF) and fractional shortening (FS) were significantly lower in the ISO group compared to the control group ($P < 0.01$); compared to the ISO group, the CRC-CDs group (1.75, 3.5 and 7 mg/kg, respectively) and Propranolol (10 mg/kg) groups showed significantly higher EF and FS ($P < 0.01$), and showed a dose dependence.

Effect of CRC-CDs on ISO-induced heart morphology and its heart index in rats

As shown in Figure 5 below, the hearts of the rats in the blank control group (Figure 5A) had a smooth surface and red colour. The hearts of the rats in the model group (Figure 5B) had a grey colour and obvious ischaemic foci were visible in the apical region. The hearts of the rats in the positive drug and CRC-CDs groups (1.75, 3.5 and 7 mg/kg, respectively) had a red and smooth appearance and improved myocardial ischaemia, especially at high doses. The results demonstrated that CRC-CDs significantly improved myocardial ischemia and showed a dose-related effect (Figure 5C–F). As shown in Figure 5G below, Compared with the control group, the heart index of rats in the model group was significantly higher ($P < 0.01$). Compared with the model group, the cardiac index of rats in the high, medium and low doses of CRC-CDs was significantly lower ($P < 0.01$). Heart index (HWI) = heart weight/body weight ratio (HW/BW).

Histopathological examination of myocardial tissue

To further investigate the protective effect of CRC-CDs on myocardial tissues, we performed histopathological examination of myocardial tissues in each group of rats using hematoxylin-eosin staining and Masson staining (Figure 6). The micrographs of the normal control group showed uniform myocardial cell morphology, normal and well-aligned myocardial fibres, no inflammatory cell infiltration or congestion and oedema. However, in the model rats (ISO group), myocardial cells were

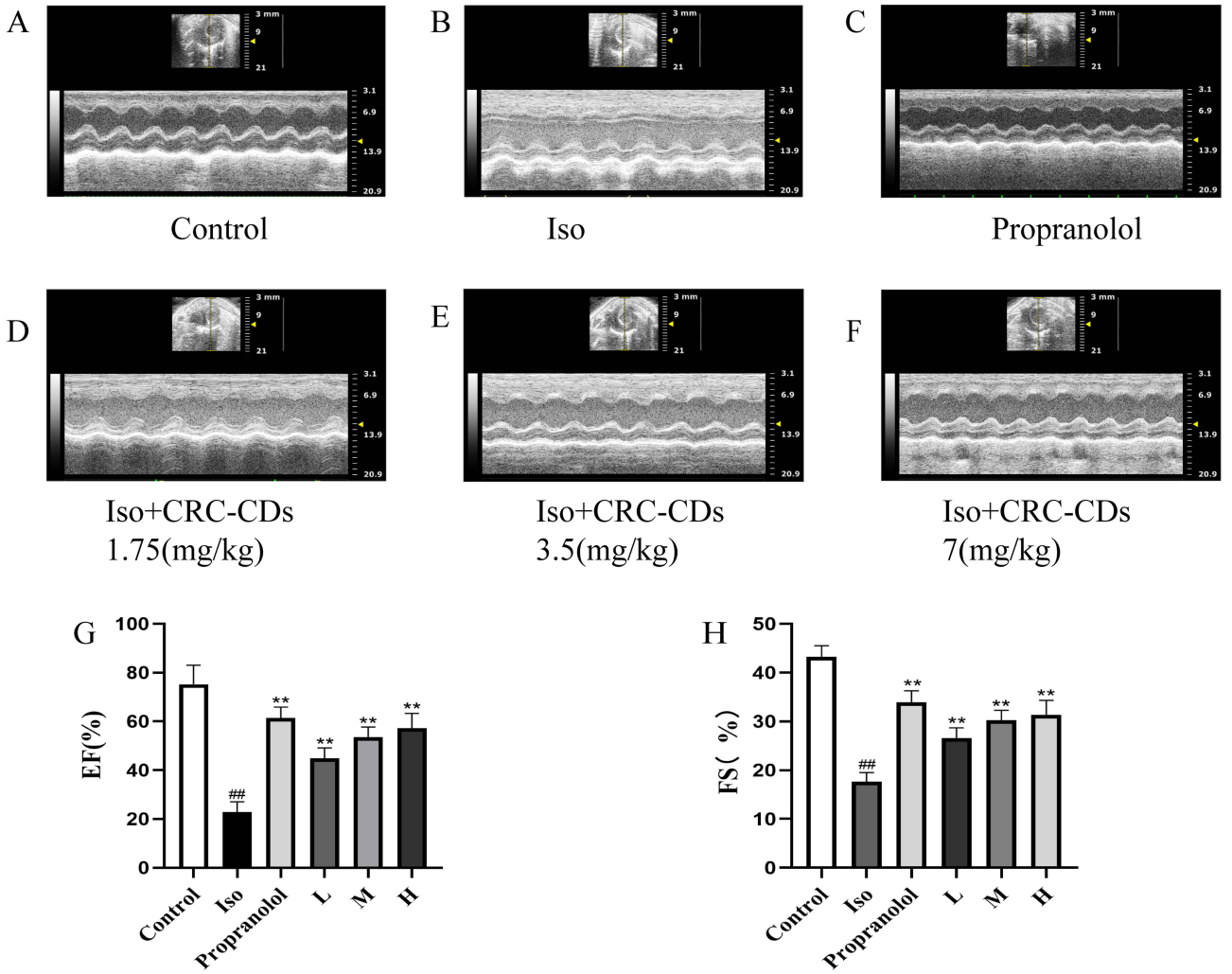

Figure 4 The echocardiographic results showed that pretreatment with CRC-CDs increased the levels of EF and FS in rats. (**A**) Control group. (**B**) Iso group. (**C**) Propranolol group. (**D**) Low-dose CRC-CDs group. (**E**) Medium-dose CRC-CDs group. (**F**) High-dose CRC-CDs group. (**G**) Left ventricular ejection fraction of rats in each group. (**H**) Left ventricular shortening fraction in all groups of rats. Date are represented as means ± SD (n = 8). $^{\#\#}P < 0.01$ compared with the control group, $^{**}P < 0.01$ compared with the Iso group.

disorganized, with interstitial edema, massive inflammatory cell infiltration and varying degrees of myocardial cell necrosis, and marked proliferation of collagen fibers and connective tissue. The results of CRC-CDs pretreatment group (1.75, 3.5 and 7mg/kg, respectively) showed regular arrangement of cardiomyocytes, some cardiomyocytes were seen to be enlarged with a small amount of inflammatory cell infiltration, and myocardial fibrosis was significantly improved compared to the model group in a dose-dependent manner, which indicated that CRC-CDs could effectively improve the histopathological changes of myocardium in ISO-induced rats. Microscopic images of the drug-positive pretreatment group showed structural integrity of the myocardium, a significant reduction in cellular infiltration and necrosis, and a marked improvement in myocardial fibrosis.

Effect of CRC-CDs on the area of ISO-induced myocardial infarction in rats

The TTC method was used to analyse the size of myocardial infarct area in each group of rats as shown in Figure 7A–G. The control rats had normal myocardial tissue (Figure 7A), no myocardial ischaemia and a red colour. However, the area of myocardial infarction in the ISO-induced model group of rats was significantly increased ($P < 0.01$), showing a large white infarct area (Figure 7B). As shown in Figure 7G below, Compared with the model group, both the positive drug and CRC-CDs pre-dose groups (3.5 and 7 mg/kg, respectively) significantly reduced ($P < 0.01$) the area of myocardial ischemic infarction and improved myocardial ischemia in rats, except for the low dose of CRC-CDs ($P < 0.05$).

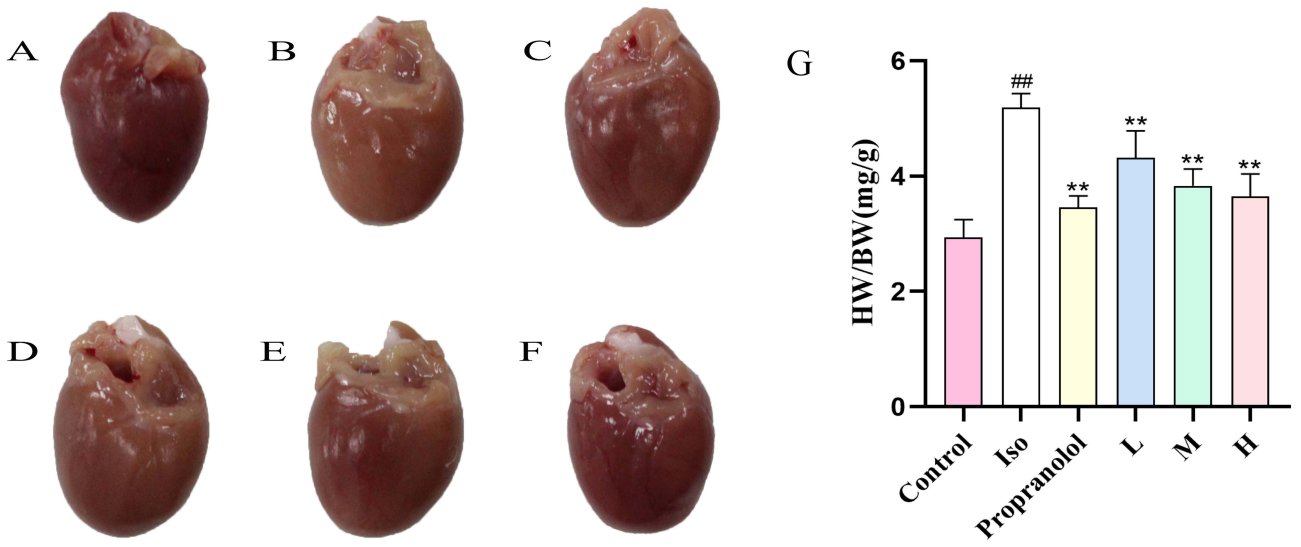

Figure 5 Pretreatment with CRC-CDs improved ISO-induced myocardial ischaemia and reduced relative heart weight in rats. (**A**) Control group. (**B**) Iso group. (**C**) Propranolol group. (**D**) Low-dose CRC-CDs group. (**E**) Medium-dose CRC-CDs group. (**F**) High-dose CRC-CDs group. (**G**) Heart index of rats in each group. Date are represented as means ± SD (n = 8). $^{\#\#}P < 0.01$ compared with the control group, $^{**}P < 0.01$ compared with the Iso group.

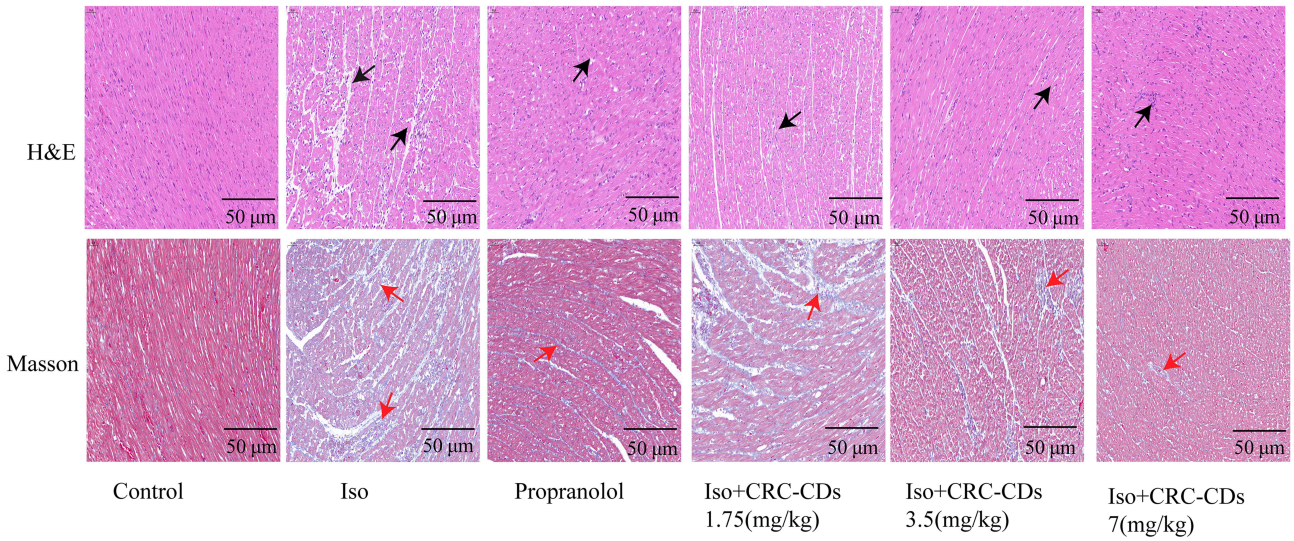

Figure 6 Histopathological changes in rat myocardium. ISO induced damage such as necrosis, edema, inflammatory cell infiltration (black arrow) and collagen fibril deposition (red arrow) in rat myocardium, whereas CRC-CDs improved the histopathological changes in rat myocardium.

Effect of CRC-CDs on ISO-induced serum cardiac marker enzymes and lipids in rats

To further investigate the cardioprotective effects of CRC-CDs, we measured the activity of myocardial biomarkers in the serum of various groups of rats, which are released into the blood during myocardial ischaemia and are commonly used to reflect the severity of heart disease. As shown in Figure 8A–D below, the serum levels of cardiac marker enzymes in the ISO group rats were significantly higher than those in the control group ($P < 0.01$). However, the positive drug group and CRC-CDs group (1.75, 3.5 and 7 mg/kg, respectively) could significantly reduce myocardial enzyme levels compared to the model group ($P < 0.01$ or $P < 0.05$), thus exerting a cardioprotective effect. The results showed that CRC-CDs could also regulate blood lipid levels in rats. As shown in Figure 8E–H, compared to the model group, CRC-CDs significantly reduced LDL, TC and TG levels and increased HDL levels in rats ($P < 0.01$ or $P < 0.05$), and the results showed the levels of AST, CK, CK-MB, and TG exhibited a dose-dependent relationship.

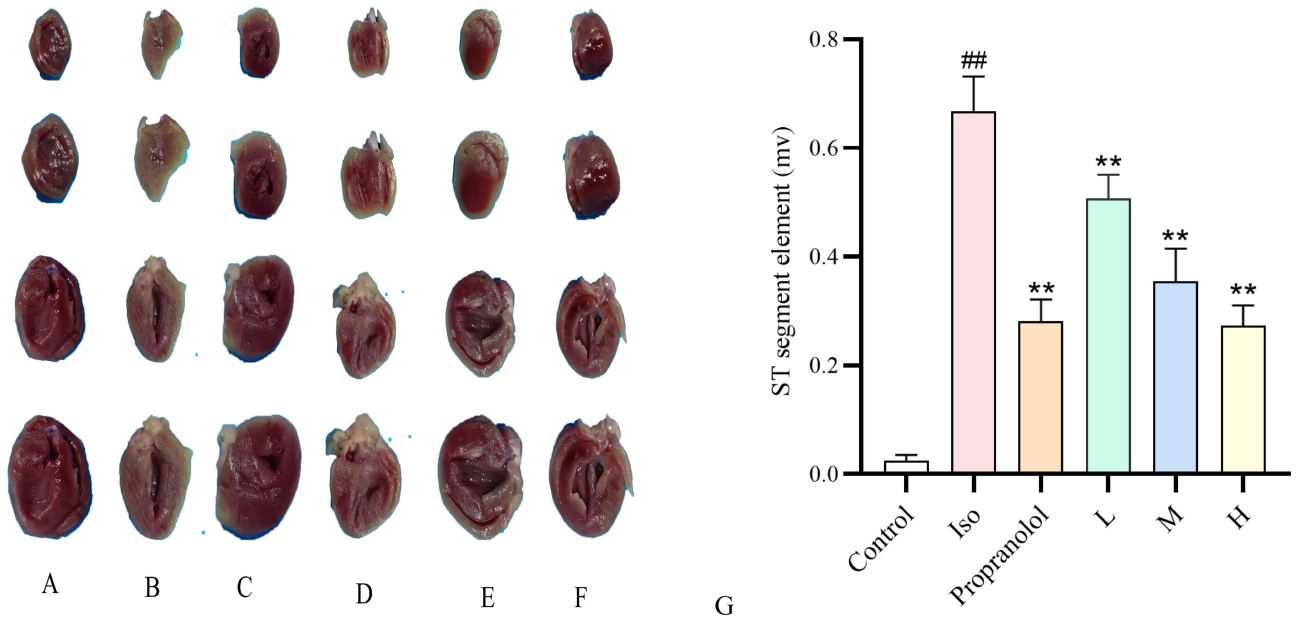

Figure 7 Photomicrographs of TTC staining of myocardial tissue from various groups of rats. (**A**) Control group. (**B**) Iso group. (**C**) Propranolol group. (**D**) Low-dose CRC-CDs group. (**E**) Medium-dose CRC-CDs group. (**F**) High-dose CRC-CDs group. (**G**) Percentage of myocardial infarct area by semi-quantification. Date are represented as means ± SD (n = 5). $^{\#\#}P < 0.01$ compared with the control group, $^{**}P < 0.01$ compared with the Iso group.

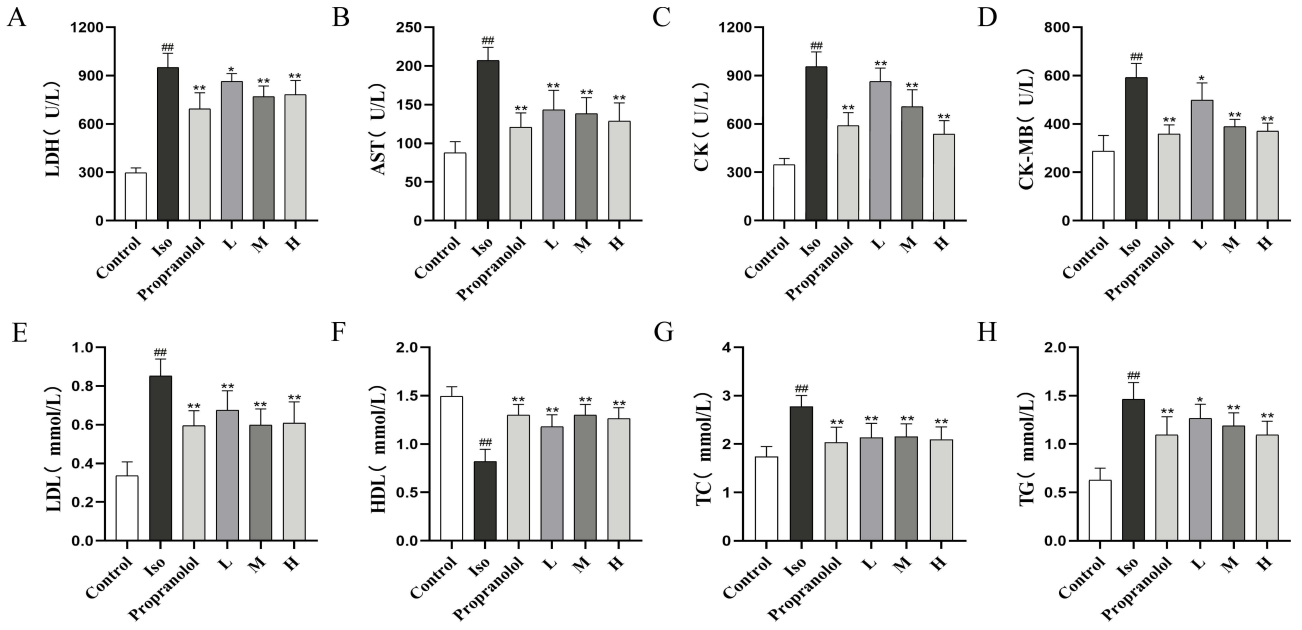

Figure 8 Effect of CRC-CDs on serum cardiac marker enzymes (**A-D**) and blood lipids (**E-H**) in various groups of rats. (**A**) LDH levels in serum. (**B**) AST levels in serum. (**C**) CK levels in serum. (**D**) CK-MB levels in serum. (**E**) LDL levels in serum. (**F**) HDL levels in serum. (**G**) TC levels in serum. (**H**) TG levels in serum. Date are represented as means ± SD (n = 8). $^{\#\#}P < 0.01$ compared with the control group, $^{**}P < 0.01$ and $^{*}P < 0.05$ compared with the Iso group.

Effect of CRC-CDs on ISO-induced myocardial antioxidant activity and Na^+-K^+-ATPase and Ca^{2+}-Mg^{2+}-ATPase activities in rats

Oxidative emergency imbalance has been shown to play an important role in the pathogenesis of AMI. Na^+-K^+-ATPase and Ca^{2+}-Mg^{2+}-ATPase are important enzymes for maintaining intracellular Ca^{2+} concentration, and their levels can indirectly reflect the degree of cardiomyocyte damage. To investigate whether the cardioprotective effects of CRC-CDs are associated with enhanced myocardial antioxidant capacity and increased Na^+-K^+/Ca^{2+}-Mg^{2+}-ATPase activity, we

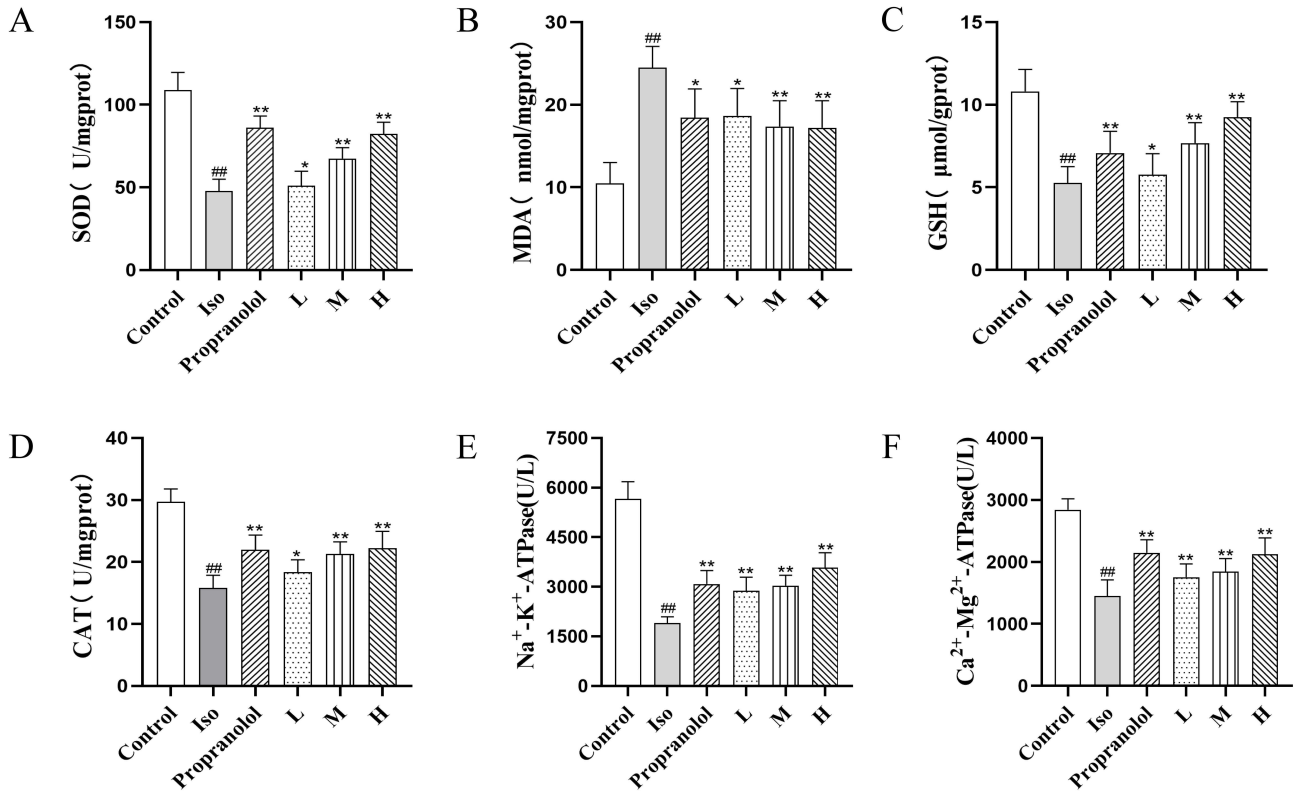

Figure 9 Effect of CRC-CDs on myocardial antioxidant activity (**A-D**) and Na^+-K^+-ATPase and Ca^{2+}-Mg^{2+}-ATPase (**E-F**) activities in various groups of rats. (**A**) SOD levels in tissues. (**B**) MDA levels in tissues. (**C**) GSH levels in tissues. (**D**) CAT levels in tissues. (**E**) Na^+-K^+-ATPase activity in tissues. (**F**) Ca^{2+}-Mg^{2+}-ATPase activity in tissues. Date are represented as means ± SD (n = 8). $^{\#\#}P<0.01$ compared with the control group, $^{**}P < 0.01$ and $^{*}P < 0.05$ compared with the Iso group.

examined oxidative stress-related parameters and ATPase activity in cardiac tissues. As shown in Figure 9A–D, lipid peroxidation products (MDA) were significantly increased in myocardial tissue of rats in the model group compared with the control group. However, cardiac antioxidant activities such as SOD, GSH and CAT were significantly reduced ($P < 0.01$). Positive drug group and CRC-CDs pretreatment group (1.75, 3.5 and 7 mg/kg, respectively) significantly reduced MDA levels while enhancing cardiac antioxidant enzymes such as SOD, GSH and CAT activities ($P < 0.01$ or $P < 0.05$). Figure 9E and F also shows that ISO-induced Na^+-K^+-ATPase and Ca^{2+}-Mg^{2+}-ATPase activities were significantly reduced ($P < 0.01$) in the model group rats, while pretreatment with CRC-CDs (1.75, 3.5 and 7 mg/kg, respectively) significantly increased the related ATPase activities and showed some dose-dependence ($P < 0.01$).

Effect of CRC-CDs on ISO-induced apoptosis in rat cardiomyocytes

The effect of CRC-CDs on ISO-induced apoptosis in rat cardiomyocytes was observed by TUNEL staining. The experimental results are shown in Figure 10. Compared with the blank control group (Figure 10A), the number of TUNEL-positive cells in the model group was significantly increased ($P < 0.01$), suggesting that the degree of apoptosis increased after ISO modeling (Figure 10B). As shown in Figure 10G below, Compared with the model group, the number of positive cardiomyocytes was significantly lower in the positive drug group and CRC-CDs (1.75, 3.5 and 7 mg/kg, respectively) pretreatment group rats ($P < 0.01$ or $P < 0.05$). The above experimental results indicated that CRC-CDs could attenuate the level of ISO-induced cardiomyocyte apoptosis in rats.

Cytotoxicity evaluation of CRC-CDs

As a potential drug material, the biosafety of CDs should be given high priority. To evaluate the cytotoxicity of CRC-CDs, H9c2 cells were exposed to a series of CRC-CDs at gradient concentrations of 15.625 ~ 1000 μg/mL for 24 h. As shown in Figure 11, when the concentration of CRC-CDs was 1000 μg/mL showed a less inhibitory effect on the cell

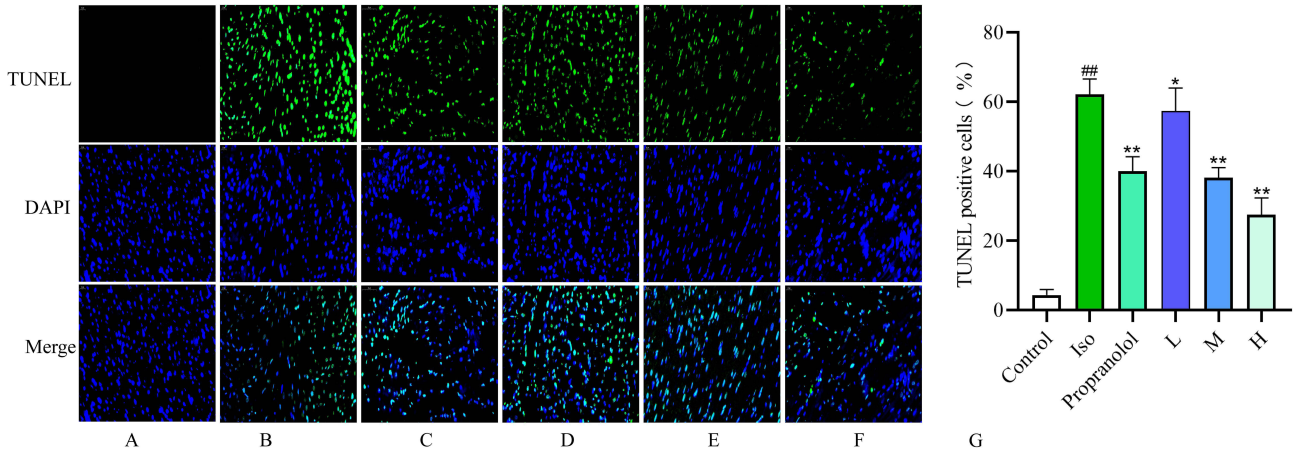

Figure 10 Apoptosis levels in different groups of rat cardiomyocytes (magnification = 400 ×, The nuclei of DAPI-positive normal cardiomyocytes fluoresced blue; the nuclei of TUNEL-positive apoptotic cardiomyocytes fluoresced green). (**A**) Control group. (**B**) Iso group. (**C**) Propranolol group. (**D**) Low-dose CRC-CDs group. (**E**) Medium-dose CRC-CDs group. (**F**) High-dose CRC-CDs group. (**G**) Percentage of TUNEL-positive cells. Date are represented as means ± SD (n = 5). $^{\#\#}P < 0.01$ compared with the control group, $^{**}P < 0.01$ and $^{*}P < 0.05$ compared with the Iso group.

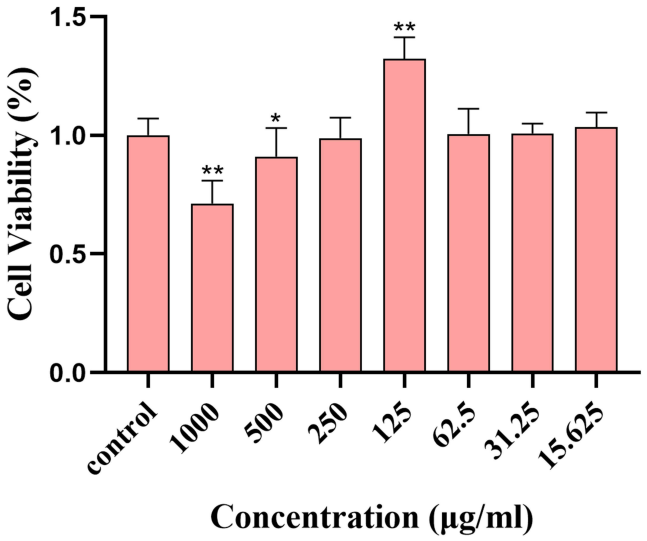

Figure 11 Effect of different concentrations of CRC-CDs on the viability of H9c2 cells. Significantly different compared to the control group at $^{**}P < 0.01$ and $^{*}P < 0.05$.

value addition, and the inhibitory effect tended to diminish as the concentration decreased. When the concentration was at 125 μg/mL promoted the value-added of cells, and as the concentration decreased, there was no significant effect on the viability of cells compared with the blank group, which indicated that CRC-CDs exhibited very low cytotoxicity.

Effect of CRC-CDs on LDH and CK levels in H9c2 cells

When cardiomyocytes are injured, the permeability of their cell membranes increases, and lactate dehydrogenase (LDH) and creatine kinase (CK) leak from the cell to the outside of the cell, which increases the level of cardiac enzymes in extracellular solution. We usually use the amount of LDH and CK released from cell cultures to reflect the degree of injury to cardiomyocytes. As shown in Figure 12A and B below, after H9c2 cells were pretreated in CRC-CDs solution for 12 h, the content of cardiac myosin level in the cell supernatant was significantly reduced compared with that of the model group and showed a certain dose-dependence, so this study preliminarily proved that CRC-CDs had a certain protective effect on cardiomyocytes.

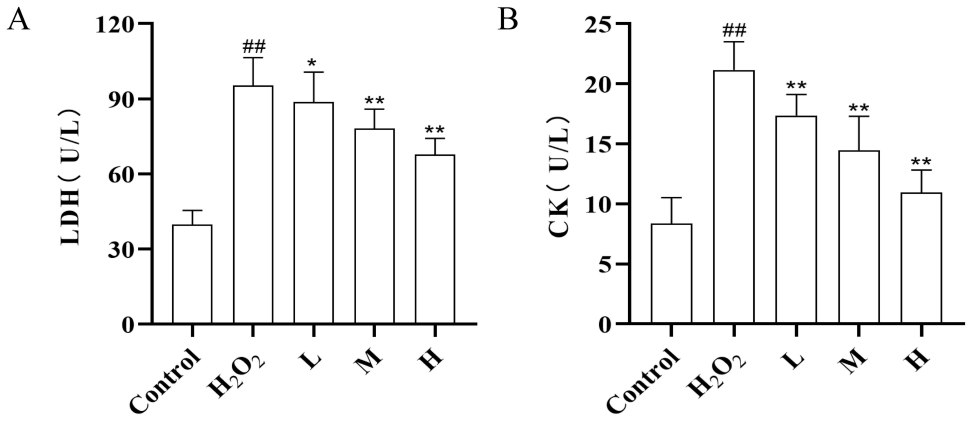

Figure 12 Effect of CRC-CDs on cardiac myosin levels in supernatants of H_2O_2-induced H9c2 cells. (**A**) LDH levels in the supernatant. (**B**) CK levels in the supernatant. Date are represented as means ± SD (n = 6). $^{\#\#}P < 0.01$ compared with the control group, $^{**}P < 0.01$ and $^{*}P < 0.05$ compared with the model group.

Discussion

As a new type of nanomaterial, CDs are receiving more and more attention and research due to their excellent properties. At present, CDs are mainly used in the medical field as an auxiliary diagnostic aid for diseases,[44] while there is a relative lack of research on their biological activity. Although our team has extracted a variety of CDs from different natural herbs in previous studies and has verified their good biological activities such as: anti-inflammatory and analgesic,[45,46] there are many important biological activities of CDs that have not yet been exploited, which deserve further exploration and research.

Curcumae Radix, a traditional herb used since ancient times for the treatment of cardiovascular diseases, is highly effective, environmentally friendly and inexpensive, and is often applied in a fire concoction, which not only increases its effectiveness but also reduces its side effects.[47] Combining the application of *Curcumae Radix* in traditional Chinese medicine and our team's previous research base, this study reveals for the first time that a novel non-toxic substance has significant anti-myocardial ischemic effects CRC-CDs with a particle size of less than 10 nm were prepared using a simple and green calcination method.

In this study, CDs were first isolated from CRC aqueous extracts and their particle size, surface functional groups and optical properties were analysed using modern spectroscopic instruments. TEM images show that the CRC-CDs are spherical, with a monodisperse quasi-spherical structure, and HRTEM images show that the CRC-CDs have a lattice spacing of 0.216 nm, with a structure similar to the crystal skeleton of graphite.[31] FTIR results showed that the surface of CRC-CDs contain polyfunctional groups such as carbonyl, hydroxyl and amino groups. The fluorescence emission spectra showed excitation at 346 nm with the highest emission peak at 455 nm, indicating that CRC-CDs are fluorescent in nature.[34] The surface elemental composition and chemical bonding of CRC-CDs were determined by XPS and the results showed that CRC-CDs are mainly composed of three elements, C, N and O, and consist of chemical bonds such as C=C/C-C, C-O/C-N, C-O, N-H and C-N. The XPS results, in conjunction with the FTIR results, indicate that the surface of CRC-CDs contains polyfunctional groups such as carbonyl, hydroxyl, and amino functional groups. The analysis of the active moieties of CRC-CDs may further explain the significant biological activity of CRC-CDs against myocardial ischaemia.[36]

Isoprenaline, a synthetic catecholamine, in excess causes excessive myocardial contraction, increased heart rate and depletion of myocardial cell energy, resulting in severe pathological structural changes in myocardial tissue.[10] High doses of ISO can lead to excessive oxidative stress in the myocardium, generating large amounts of ROS, damaging the body's antioxidant defence system and eventually leading to apoptotic necrosis due to ischaemia and hypoxia in the myocardial cells.[48] Since the ISO-induced AMI model is similar to the clinical patient onset and has the advantages of simplicity and convenience, low animal mortality and model stability, this study used an ISO-induced animal model to study the cardioprotective effects of CRC-CDs. In addition, the β-adrenergic receptor antagonist Propranolol was used as a positive control.[49]

In cardiac disease, ECG is the most commonly used clinical test. When AMI occurs, there are specific changes in the ST segment of the ECG, so the magnitude of ST segment changes can basically reflect the severity of myocardial

infarction. Echocardiography is also an important tool for detecting cardiac function.[50] The ejection fraction (EF) and shortening fraction (FS) in echocardiography are often used as important indicators of cardiac function, with EF and FS falling below normal values when ischaemic damage to the myocardium occurs.[51] In this study, we found that the rats in the model group had significantly elevated ECG ST segments (> 0.2mv) and significantly reduced EF and FS. In contrast, CRC-CDs significantly reduced the elevation of ECG ST segment and significantly increased EF and FS values after two weeks of pre-administration. Both EF and FS outcomes demonstrate that across all dosage levels of CRC-CDs, there is a notable enhancement in cardiac ejection function, with the most pronounced improvement observed at the highest dosage, confirming a clear dose-dependent efficacy. The results showed that CRC-CDs have positive inotropic effects and can reduce the damage to myocardium caused by ISO.

When myocardial ischemic infarction occurs, the functional integrity of the myocardial cells is damaged and the permeability of the cell membrane increases leading to a massive release of intracellular AST, LDH, CK, CK-MB and other cardiac enzymes into the bloodstream.[52] Therefore, measurement of serum levels of cardiac enzymes is usually indicative of the severity of cardiomyopathy. The results showed that the serum levels of cardiac enzymes in the ISO group of rats were significantly increased, whereas the levels of cardiac enzymes in the CRC-CDs pretreatment group were significantly downregulated, indicating that CRC-CDs could effectively limit the leakage of these enzymes to the extracellular level and maintain the functional integrity of cardiac myocyte.[53] Histopathological sections further demonstrated that ISO caused disorganized myocardial fibre arrangement, structural and functional damage to myocardial cells, interstitial oedema and massive inflammatory cell infiltration with marked collagen fibrillation in rats, which was significantly reduced by pretreatment with CRC-CDs.[11] Additionally, CRC-CDs demonstrated a dose-dependent reduction in myocardial cell damage induced by isoproterenol, with the optimal alleviation observed at the highest dosage.

Inadequate energy supply is an important factor in myocardial cell injury. Increased intracellular Ca^{2+} concentration in the myocardium can increase myocardial contractility and oxygen demand, and excessive myocardial contraction can lead to ATP degradation, ultimately leading to myocardial cell injury.[50] The Na^{+}-K^{+}-ATPase and Ca^{2+}-Mg^{2+}-ATPase in the cardiomyocyte membrane play an important role in maintaining intracellular Ca^{2+} concentration, and their reduced activity can cause intracellular Ca^{2+} overload and consequently apoptosis in cardiomyocytes.[54] ISO mediates phosphorylation of calcium channels by activating the adenylate cyclase-cyclic adenosine monophosphate-protein kinase A (AC-cAMP-PKA) signaling pathway, which in turn increases Ca^{2+} inward flow leading to calcium overload.[30] In addition, dyslipidemia is the most common risk factor for the development of myocardial infarction. Abnormal lipid metabolism leads to the deposition of lipids in the intima of arteries, which in turn promotes the development of myocardial infarction.[48,55] In this study, myocardial Na^{+}- k^{+}-ATPase and Ca^{2+}- Mg^{2+}-ATPase activities were significantly reduced in the ISO injection group alone, while ATPase activities were significantly increased in the CRC-CDs pre-administered group. The serum results showed that CRC-CDs significantly reduced LDL, TC and TG levels and increased HDL levels in rats, and the reduction in lipid levels may be related to the elevated ATPase activity of the body, and the levels of AST, CK, CK-MB, and TG show dose-dependence, The levels of AST, CK, CK-MB, and TG, along with ATPase, collectively demonstrated dose-dependent characteristics. Although a few indicators (as shown in Figure 8, A-LDH, E-LDL, F-HDL, G-TC) did not exhibit the ideal dose-dependent relationship, the pharmacological effects of the medium and high dose groups were superior to those of the low dose group, and there were no significant differences between the medium and high dose groups ($P > 0.05$), Hence, it can be inferred that these biomarkers retain their dose-dependent nature, and this pattern may be more distinctly observable across a wider concentration spectrum.

Oxidative stress and apoptosis play an important role in the pathogenesis of AMI.[56] High doses of ISO induce ROS-mediated lipid peroxidation, thereby enhancing the oxidative stress response in cardiomyocytes through hypoxia, calcium overload and cardiomyocyte membrane loss.[57] Cardiac myocytes produce large amounts of ROS under ischaemic and hypoxic conditions, which cause oxidative damage to proteins and DNA within the cell membrane and ultimately lead to changes in energy metabolism, which in turn cause cell necrosis and apoptosis.[11] MDA, a marker of oxidative stress resulting from the peroxidation of polyunsaturated fatty acids, can accumulate in the myocardium as a result of acute ischemic injury.[58] Free radical scavenging enzymes such as SOD, MDA, GSH and CAT are the first line of defence of the antioxidant system.[59] SOD is usually found in the plasma membrane and its reduced levels are a significant marker of oxidative stress.[30] GSH protects cell membranes from oxidative damage by reducing hydrogen peroxide and lipid

peroxidation. CAT is a tetrameric haemoglobin that acts as a catalyst for the removal of hydrogen peroxide.[50] Studies have shown that CRC-CDs can increase the activity of antioxidant enzymes in vivo by increasing SOD, GSH and CAT levels and decreasing MDA levels to counteract free radical-induced lipid peroxidation and protect ischemic cardiomyocytes. The three enzymes work synergistically in the antioxidant system to eliminate oxygen free radicals, reduce the peroxidation of cellular membrane lipids, and mitigate damage to cardiomyocytes. All dosage groups of CRC-CDs demonstrated good antioxidant effects, with a dose-dependent manner and the highest dosage showing the best results, indicating that the higher the concentration of CRC-CDs, the stronger the antioxidant capacity. The TUNEL staining results also confirmed that CRC-CDs inhibited ISO-induced cardiomyocyte apoptosis to exert cardioprotective effects.

Conclusion

In summary, CDs were first isolated from *Curcumae Radix* Carbonisata aqueous extracts and their particle size, surface functional groups and optical properties were analysed using modern spectroscopic instruments. In addition, this study investigated the protective effect of CRC-CD_S against isoproterenol (ISO)-induced myocardial infarction (MI) in rats and its mechanism. The results of the study showed that CRC-CDs, when pre-administered, could reduce the serum levels of cardiac enzymes and increase the antioxidant capacity of myocardial tissues in model rats, and the mechanism of action may be related to the reduction of excessive oxidative stress and cardiomyocyte apoptosis in myocardial tissues. CRC-CDs has the potential for clinical application as an anti-myocardial ischemia drug candidate, which not only provides evidence for further broadening the biological application of cardiovascular diseases, but also offers potential hope for the application of nanomedicine to treat intractable diseases.

Acknowledgment

We greatly appreciate the support of the Special Funds for Fundamental Research Expenses of Central Universities (China, 2019-JYB-TD-001) and Grant for Qihuang Scholars of the State Administration of Traditional Chinese Medicine (China, 90020163320012).

Disclosure

The authors report no conflicts of interest in this work.

References

1. Yang MJ, Linn BS, Zhang YM, Ren J. Mitophagy and mitochondrial integrity in cardiac ischemia-reperfusion injury. *Biochim Biophys Acta-Mol Basis Dis*. 2019;1865(9):2293–2302. doi:10.1016/j.bbadis.2019.05.007
2. Song JL, Murugiah K, Hu S, et al. Incidence, predictors, and prognostic impact of recurrent acute myocardial infarction in China. *Heart*. 2021;107(4):313–318. doi:10.1136/heartjnl-2020-317165
3. Solomon R, Nowak R, Hudson M, Moyer M, Jacobsen G, McCord J. Is duration of symptoms predictive of acute myocardial infarction? *Curr Probl Cardiol*. 2021;46(3):100555. doi:10.1016/j.cpcardiol.2020.100555
4. Su Q, Liu Y, Lv XW, Dai RX, Yang XH, Kong BH. LncRNA TUG1 mediates ischemic myocardial injury by targeting miR-132-3p/HDAC3 axis. *Am J Physiol -Heart Circul Physiol*. 2020;318(2):H332–H344. doi:10.1152/ajpheart.00444.2019
5. Mo XY, Zhao NN, Du XY, Bai LY, Liu JK. The protective effect of peony extract on acute myocardial infarction in rats. *Phytomedicine*. 2011;18(6):451–457. doi:10.1016/j.phymed.2010.10.003
6. Bai YD, Yang YR, Mu XP, et al. Hydrogen sulfide alleviates acute myocardial ischemia injury by modulating autophagy and inflammation response under oxidative stress. *Oxid Med Cell Longev*. 2018;2018:3402809. doi:10.1155/2018/3402809
7. Hundahl LA, Sattler SM, Skibsbye L, Diness JG, Tfelt-Hansen J, Jespersen T. Pharmacological blockade of small conductance Ca2+-activated K+ channels by ICA reduces arrhythmic load in rats with acute myocardial infarction. *Pflugers Arch*. 2017;469(5–6):739–750. doi:10.1007/s00424-017-1962-6
8. Alexopoulos D. Acute myocardial infarction late following stent implantation: incidence, mechanisms and clinical presentation. *Int J Cardiol*. 2011;152(3):295–301. doi:10.1016/j.ijcard.2011.01.017
9. Thiele H, Ohman EM, deWaha-Thiele S, Zeymer U, Desch S. Management of cardiogenic shock complicating myocardial infarction: an update 2019. *Eur Heart J*. 2019;40(32):2671–+. doi:10.1093/eurheartj/ehz363
10. Zheng B, Qi JY, Yang YK, et al. Mechanisms of cinnamic aldehyde against myocardial ischemia/hypoxia injury in vivo and in vitro: involvement of regulating PI3K/AKT signaling pathway. *Biomed Pharmacother*. 2022;147:112674. doi:10.1016/j.biopha.2022.112674
11. Jiang TC, Han FL, Gao GY, Liu M. Mangiferin exert cardioprotective and anti-apoptotic effects in heart failure induced rats. *Life Sci*. 2020;249:117476. doi:10.1016/j.lfs.2020.117476
12. Ke QJ, Liu F, Tang YX, et al. The protective effect of isosteviol sodium on cardiac function and myocardial remodelling in transverse aortic constriction rat. *J Cell Mol Med*. 2021;25(2):1166–1177. doi:10.1111/jcmm.16182

13. Ashuri M, Moztarzadeh F, Nezafati N, Hamedani AA, Tahriri M. Development of a composite based on hydroxyapatite and magnesium and zinc-containing sol-gel-derived bioactive glass for bone substitute applications. *Mater Sci Eng C-Mater Biol Appl*. 2012;32(8):2330–2339. doi:10.1016/j.msec.2012.07.004
14. Bonifacio BV, da Silva PB, Ramos MAD, Negri KMS, Bauab TM, Chorilli M. Nanotechnology-based drug delivery systems and herbal medicines: a review. *Int J Nanomed*. 2014;9:1–15.
15. Parveen S, Misra R, Sahoo SK. Nanoparticles: a boon to drug delivery, therapeutics, diagnostics and imaging. *Nanomed-Nanotechnol Biol Med*. 2012;8(2):147–166. doi:10.1016/j.nano.2011.05.016
16. Gomes SLR, Dias A, Silva MMS, Silva BVM, Dutra RF. A carbon nanotube-based electrochemical immunosensor for cardiac troponin T. *Microchem J*. 2013;109:10–15. doi:10.1016/j.microc.2012.05.033
17. Abdorahim M, Rabiee M, Alhosseini SN, et al. Nanomaterials-based electrochemical immunosensors for cardiac troponin recognition: an illustrated review. *Trac-Trends Anal Chem*. 2016;82:337–347. doi:10.1016/j.trac.2016.06.015
18. Cui WG, Wang AJ, Zhao C, Zhu WQ. Editorial: nanotechnology in Cardiovascular Regenerative Medicine. *Front Bioeng Biotechnol*. 2020;8:608844. doi:10.3389/fbioe.2020.608844
19. Chintapula U, Chikate T, Sahoo D, et al. Immunomodulation in age-related disorders and nanotechnology interventions. *Wiley Interdiscip Rev - Nanomed Nanobiotech*. 2022;15(1):e1840. doi:10.1002/wnan.1840
20. Wang YJ, Chen J, Liu LM, et al. Novel metal doped carbon quantum dots/CdS composites for efficient photocatalytic hydrogen evolution. *Nanoscale*. 2019;11(4):1618–1625. doi:10.1039/C8NR05807E
21. Hu JJ, Zhu Y, Song HJ, Wang Y, Shan Y. Electrochemiluminescence from CdS Nanocrystals@Carbon Dots Composite Film. *Chin J Inorg Chem*. 2020;36(2):324–332.
22. Luo WK, Zhang LL, Yang ZY, et al. Herbal medicine derived carbon dots: synthesis and applications in therapeutics, bioimaging and sensing. *J Nanobiotechnol*. 2021;19(1):320. doi:10.1186/s12951-021-01072-3
23. Zhang Y, Wang SN, Lu F, et al. The neuroprotective effect of pretreatment with carbon dots from crinis carbonisatus (carbonized human hair) against cerebral ischemia reperfusion injury. *J Nanobiotechnol*. 2021;19(1):257. doi:10.1186/s12951-021-00908-2
24. Zhang ML, Cheng JJ, Zhang Y, et al. Green synthesis of Zingiberis rhizoma-based carbon dots attenuates chemical and thermal stimulus pain in mice. *Nanomedicine*. 2020;15(9):851–869. doi:10.2217/nnm-2019-0369
25. Lu F, Ma YR, Huang H, et al. Edible and highly biocompatible nanodots from natural plants for the treatment of stress gastric ulcers. *Nanoscale*. 2021;13(14):6809–6818. doi:10.1039/D1NR01099A
26. Lu F, Song YX, Huang H, et al. Fluorescent carbon dots with tunable negative charges for bio-imaging in bacterial viability assessment. *Carbon*. 2017;120:95–102. doi:10.1016/j.carbon.2017.05.039
27. Zhao Y, Lu F, Zhang Y. Water-soluble carbon dots in cigarette mainstream smoke: their properties and the behavioural, neuroendocrinological, and neurotransmitter changes they induce in mice. *Int J Nanomed*. 2021;16:2203–2217. doi:10.2147/IJN.S291670
28. Tao WY, Xu X, Wang X, et al. Network pharmacology-based prediction of the active ingredients and potential targets of Chinese herbal Radix Curcumae formula for application to cardiovascular disease. *J Ethnopharmacol*. 2013;145(1):1–10. doi:10.1016/j.jep.2012.09.051
29. Bei W, Jing L, Chen N. Cardio protective role of wogonin loaded nanoparticle against isoproterenol induced myocardial infarction by moderating oxidative stress and inflammation. *Colloid Surf B-Biointerfaces*. 2020;185:110635. doi:10.1016/j.colsurfb.2019.110635
30. Zhang TP, Dang MY, Zhang WZ, Lin X. Gold nanoparticles synthesized from Euphorbia fischeriana root by green route method alleviates the isoprenaline hydrochloride induced myocardial infarction in rats. *J Photochem Photobiol B-Biol*. 2020;202:111705. doi:10.1016/j.jphotobiol.2019.111705
31. Stobinski L, Lesiak B, Malolepszy A, et al. Graphene oxide and reduced graphene oxide studied by the XRD, TEM and electron spectroscopy methods. *J Electron Spectrosc Relat Phenom*. 2014;195:145–154. doi:10.1016/j.elspec.2014.07.003
32. Liu YL, Thibodeaux D, Gamble G, Bauer P, VanDerveer D. Comparative investigation of Fourier transform infrared (FT-IR) spectroscopy and X-ray diffraction (XRD) in the determination of cotton fiber crystallinity. *Appl Spectrosc*. 2012;66(8):983–986. doi:10.1366/12-06611
33. Lu WY, Li N, Chen WX, Yao YY. The role of multiwalled carbon nanotubes in enhancing the catalytic activity of cobalt tetraaminophthalocyanine for oxidation of conjugated dyes. *Carbon*. 2009;47(14):3337–3345. doi:10.1016/j.carbon.2009.07.055
34. Wei XJ, Li L, Liu JL, et al. Green synthesis of fluorescent carbon dots from gynostemma for bioimaging and antioxidant in zebrafish. *ACS Appl Mater Interfaces*. 2019;11(10):9832–9840. doi:10.1021/acsami.9b00074
35. Atchudan R, Edison T, Chakradhar D, Perumal S, Shim JJ, Lee YR. Facile green synthesis of nitrogen-doped carbon dots using Chionanthus retusus fruit extract and investigation of their suitability for metal ion sensing and biological applications. *Sensor Actuat B-Chem*. 2017;246:497–509. doi:10.1016/j.snb.2017.02.119
36. Zhang ML, Cheng JJ, Hu J, et al. Green phellodendri Chinensis cortex-based carbon dots for ameliorating imiquimod-induced psoriasis-like inflammation in mice. *J Nanobiotechnol*. 2021;19(1):105. doi:10.1186/s12951-021-00847-y
37. Carvalho A, Costa MCF, Marangoni VS, Ng PR, Nguyen TLH, Neto AHC. The degree of oxidation of graphene oxide. *Nanomaterials*. 2021;11(3):560. doi:10.3390/nano11030560
38. Yamada Y, Kim J, Matsuo S, Sato S. Nitrogen-containing graphene analyzed by X-ray photoelectron spectroscopy. *Carbon*. 2014;70:59–74. doi:10.1016/j.carbon.2013.12.061
39. Rosenthal D, Ruta M, Schlogl R, Kiwi-Minsker L. Combined XPS and TPD study of oxygen-functionalized carbon nanofibers grown on sintered metal fibers. *Carbon*. 2010;48(6):1835–1843. doi:10.1016/j.carbon.2010.01.029
40. Martin TN, Groenning BA, Murray HM, et al. ST-segment deviation analysis of the admission 12-lead electrocardiogram as an aid to early diagnosis of acute myocardial infarction with a cardiac magnetic resonance imaging gold standard. *J Am Coll Cardiol*. 2007;50(11):1021–1028. doi:10.1016/j.jacc.2007.04.090
41. Nestelberger T, Cullen L, Lindahl B, et al. Diagnosis of acute myocardial infarction in the presence of left bundle branch block. *Heart*. 2019;105(20):1559–1567. doi:10.1136/heartjnl-2018-314673
42. Galasko GIW, Basu S, Lahiri A, Senior R. Is echocardiography a valid tool to screen for left ventricular systolic dysfunction in chronic survivors of acute myocardial infarction? A comparison with radionuclide ventriculography. *Heart*. 2004;90(12):1422–1426. doi:10.1136/hrt.2003.027425

43. Dwivedi G, Janardhanan R, Hayat SA, Lim TK, Senior R. Improved prediction of outcome by contrast echocardiography determined left ventricular remodelling parameters compared to unenhanced echocardiography in patients following acute myocardial infarction. *Eur J Echocardiogr*. 2009;10(8):933–940. doi:10.1093/ejechocard/jep099
44. Lv A, Chen Q, Zhao C, et al. Long-wavelength (red to near-infrared) emissive carbon dots: key factors for synthesis, fluorescence mechanism, and applications in biosensing and cancer theranostics. *Chin Chem Lett*. 2021;32(12):3653–3664. doi:10.1016/j.cclet.2021.06.020
45. Wu JS, Zhang ML, Cheng JJ, et al. Effect of lonicerae japonicae flos carbonisata-derived carbon dots on rat models of fever and hypothermia induced by lipopolysaccharide. *Int J Nanomed*. 2020;15:4139–4149. doi:10.2147/IJN.S248467
46. Zhao YS, Zhang Y, Kong H, Cheng GL, Qu HH, Zhao Y. Protective effects of carbon dots derived from armeniacae semen amarum carbonisata against acute lung injury induced by lipopolysaccharides in rats. *Int J Nanomed*. 2022;17:1–14. doi:10.2147/IJN.S338886
47. Ao MY, Li X, Liao YJ, et al. Curcumae Radix: a review of its botany, traditional uses, phytochemistry, pharmacology and toxicology. *J Pharm Pharmacol*. 2022;74(6):779–792. doi:10.1093/jpp/rgab126
48. Feriani A, Khdhiri E, Tir M, et al. (E)-N '-(1-(7-Hydroxy-2-Oxo-2H-Chromen-3-Yl) Ethylidene) Benzohydrazide, a Novel Synthesized Coumarin, Ameliorates Isoproterenol-Induced Myocardial infarction in rats through Attenuating Oxidative Stress, Inflammation, and Apoptosis. *Oxid Med Cell Longev*. 2020;2020:2432918. doi:10.1155/2020/2432918
49. Zhang HW, Chen HY, Li J, et al. Hirudin protects against isoproternol-induced myocardial infraction by alleviating oxidative via an Nrf2 dependent manner. *Int J Biol Macromol*. 2020;162:425–435. doi:10.1016/j.ijbiomac.2020.06.097
50. Fan SR, Zhang JF, Xiao Q, et al. Cardioprotective effect of the polysaccharide from Ophiopogon japonicus on isoproterenol-induced myocardial ischemia in rats. *Int J Biol Macromol*. 2020;147:233–240. doi:10.1016/j.ijbiomac.2020.01.068
51. Wang DD, Lv LY, Xu Y, et al. Cardioprotection of panax notoginseng saponins against acute myocardial infarction and heart failure through inducing autophagy. *Biomed Pharmacother*. 2021;136:111287. doi:10.1016/j.biopha.2021.111287
52. Lu Y, Yang ML, Peng MZ, et al. Kuanxiong aerosol inhibits apoptosis and attenuates isoproterenol-induced myocardial injury through the mitogen-activated protein kinase pathway. *J Ethnopharmacol*. 2021;269:113757. doi:10.1016/j.jep.2020.113757
53. Yang YN, Ding ZH, Zhong RX, et al. Cardioprotective effects of a fructus aurantii polysaccharide in isoproterenol-induced myocardial ischemic rats. *Int J Biol Macromol*. 2020;155:995–1002. doi:10.1016/j.ijbiomac.2019.11.063
54. Meeran MFN, Azimullah S, Adeghate E, Ojha S. Nootkatone attenuates myocardial oxidative damage, inflammation, and apoptosis in isoproterenol-induced myocardial infarction in rats. *Phytomedicine*. 2021;84:153405. doi:10.1016/j.phymed.2020.153405
55. Tao HJ, Yang XY, Wang WX, et al. Regulation of serum lipidomics and amino acid profiles of rats with acute myocardial ischemia by salvia miltiorrhiza and panax notoginseng herb pair. *Phytomedicine*. 2020;67:153162. doi:10.1016/j.phymed.2019.153162
56. Yang C, Zhang Y, Yang BF. MIAT, a potent CVD-promoting lncRNA. *Cell Mol Life Sci*. 2022;79(1):43. doi:10.1007/s00018-021-04046-8
57. Geng ZH, Huang L, Song MB, Song YM. Protective effect of a polysaccharide from Salvia miltiorrhiza on isoproterenol (ISO)-induced myocardial injury in rats. *Carbohydr Polym*. 2015;132:638–642. doi:10.1016/j.carbpol.2015.06.086
58. Viswanadha VP, Dhivya V, Beeraka NM, et al. The protective effect of piperine against isoproterenol-induced inflammation in experimental models of myocardial toxicity. *Eur J Pharmacol*. 2020;885:173524. doi:10.1016/j.ejphar.2020.173524
59. Zhao TJ, Wu W, Sui LH, et al. Reactive oxygen species-based nanomaterials for the treatment of myocardial ischemia reperfusion injuries. *Bioact Mater*. 2022;7:47–72. doi:10.1016/j.bioactmat.2021.06.006